Evaluation of micro-hologram activation for dynamic display applications

Matthias Colard, Fabian Rainouard, Olivier Haeberle, Chrisophe Martinez

Research Article | Vol. 32, No. 17 / 12 Aug 2024 / Optics Express 30144
Optics EXPRESS

Evaluation of micro-hologram activation for dynamic display applications

MATTHIAS COLARD,[1,2] FABIAN RAINOUARD,[1,2,3] OLIVIER HAEBERLE,[2] AND CHRISOPHE MARTINEZ[1,*]

[1] Univ. Grenoble Alpes, CEA, Leti, F-38000 Grenoble, France
[2] IRIMAS UR UHA 7499, Université de Haute-Alsace, 68093 Mulhouse, France
[3] Univ. Grenoble Alpes, Laboratoire Jean Kuntzmann, 38041 Grenoble, France
[*] christophe.martinez@cea.fr

Abstract: We explore the implementation of dynamic behavior in holographic displays through the activation of static elementary holograms. This research takes place in an ambitious concept of near-eye display, free of any focusing optical system. We investigate the dynamic addressing of holographic elements with a size of about 27 µm, distributed on centimeter-size samples. We project dynamic images with a resolution of 10×10 pixels. This first demonstration validates the ability to activate pixelated holograms with low cross talk, with an SNR of about 26. We project various images and analyze their rendering in an optical scheme consistent with visual behavior, using the integration time of a camera to mimic visual persistence. We demonstrate the image projection in a free space optical set-up using an SLM. This demonstration may pave the way to further potential developments implementing photonic integrated circuits inside the display.

1. Introduction

Implemented at the end of the sixties with the development of lasers, holography quickly brought astonishing imaging properties, soon associated in the public with magical three-dimensional representations of reality [1]. The term holography has then evolved and is now often misused to describe a large class of imaging applications related to the general field of volumetric display [2–4]. The initial principle of holography, which involves recording the phase and amplitude of a wave in a photosensitive material, has also evolved with the advent of computing technologies. The association of sampling and holography is the basis of the concept of computer-generated holograms (CGHs), it has led to the development of various technologies we can classify into two groups. The first one can be described as dynamic digital holography; it concerns the computing of images through their Fourier transform and their reproduction with the use of a spatial light modulator (SLM). It is now widely used in various holographic display technologies, in particular with the recent development of augmented and mixed reality (AR/MR) [5–7]. The second group of technologies, which we can describe as static digital holography, uses analog material to record complex optical functions generated by a computer. It was first implemented with a lithographic recording process through the development of CGHs [8,9]. Recently, it has found new ways of implementation with the development of holographic printers for ultra-realistic imaging or holographic optical elements design [10–12].

Dynamic digital holography is of particular interest for AR/MR applications as it allows holographic image projection in an interactive way. However, due to the use of SLM, the imaging performance is strongly constrained by diffraction issues [13]. On the other hand, due to the use of analog photo-material, static digital holography is less impacted by diffraction issues. However, its static behavior restricts its use to a limited range of applications. Some research groups have investigated dynamic schemes for analog holography, but they are limited to the commutation of optical function and, in the case of imaging, constrained by low material response time [14–17].

#527754 https://doi.org/10.1364/OE.527754
Journal © 2024 Received 13 May 2024; revised 25 Jun 2024; accepted 25 Jun 2024; published 6 Aug 2024

Optics EXPRESS

A few years ago, we proposed an original concept of a holographic near-eye display (NED) system based on the activation of holographic pixels for AR applications [18]. The use of holography in association with photonics integrated circuit (PIC) could allow, in our study case, for the development of an AR device free of any optical projection systems. It could respond to the form factor issue, which represents a current bottleneck for the adoption of this device for the consumers. Part of this research investigates how one can implement dynamic behavior in analog holographic photo-material to get rid of diffraction issues while allowing interactive applications. It locates this project at the frontier of dynamic and static digital holography.

The concept of sampling is crucial in digital holography, and a focus on the sampling element helps in understanding the various approaches presented in this contribution. In the general case of a display, the "pixel" refers to the "picture element"; it encodes the localized amplitude of the image. In the case of CGHs, the digital hologram is the result of a computation algorithm, and we use the same term "pixel" to describe the sampling element. It mainly relates to a phase element and encodes one information: the localized phase value of the CGH. If implemented with a liquid crystal on silicon (LCoS) SLM, it corresponds to the localized refractive index variation of the liquid crystal [19]. In the case of holographic printers, the sampling element is an elementary hologram that encodes various complex information. We use the term "hogel" to describe this sampling element. When recorded with an SLM, the hogel contains all the information generated by the SLM pixels. In our concept, the sampling element encodes two pieces of information: the localized angle and phase of the wavefront. It corresponds to the elementary pattern of the interference fringes that form the hologram. So, it is for the hologram what the pixel is for the image: its smallest, elementary part, and we introduce the term "hoel" to describe this "hologram element". It is relevant to emphasize the difference between the two concepts of "hogel" and "hoel": while the hogel is in itself a hologram, as it includes a complex phase and amplitude function, with a size of about a few hundred microns, our sampling element is a Bragg grating, with a size of a few tens of microns.

Extending the concept of a pixel in a display with the hoel in a hologram, we could introduce interactive behavior in the hologram recovery process by independently modulating each hoel recovery. This could allow the development of a disruptive concept of displays based on self-focusing imaging [18]. In this paper, a first insight into this approach of hoel activation is described.

2. Methods

2.1. Hologram recording and recovery

The principle of the hoels recording process is summarized in Fig. 1(a) and is described in more detail in a former publication [20]. An object beam, coding the angular direction of a pixel in the far field, is divided into various optical beams projected onto the surface of the sample, following a given distribution. On the other side of the sample, a reference beam is also divided and projected with the same distribution. The reference beam distribution is aligned with the object beam distribution and is kept normal to the surface of the sample. A distribution of hoels is recorded at the location of the beams overlaps. After the recording, the sample is shifted and another recording is proceeded, with a new object beam angular direction. At the end of the recording process, the sample is made up of a distribution of pixelated holograms (DPH).

To recover the pixelated holograms, we can use two different strategies. The first consists in using a structured reading beam to illuminate specific hoels distributions as represented in Fig. 1(b). The other strategy which is not studied here consists of using a uniform beam to activate the whole DPH.

As the DPH is recovered, we generate the corresponding angular directions and project pixels in the far field. If located near the eye, the sample projects an image onto the retina without any additional optical system. The DPH is the core of the display concept we investigate, and

Optics EXPRESS

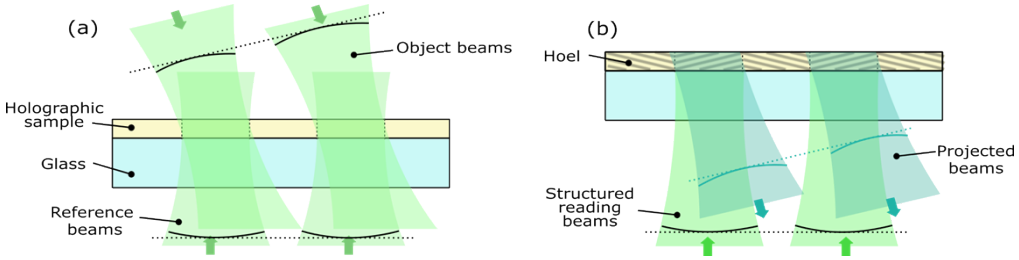

Fig. 1. (a) Schematic representation of the writing process of the pixelated holograms. Representation of the reading process (b) in the case where a structured reading beam is used, permitting to address specific DPH.

its efficiency strongly depends on the choice of the distributions [18]. We have demonstrated this unconventional imaging process with a sparse aperture distribution experiment in a former contribution [21]. This first experimental evaluation highlights the need for random distributions of hoels and DPHs to minimize diffraction issues. In this work, we evaluate the recovery of DPH in a dynamic behavior. Due to manufacturing issues related to our holographic printer, this evaluation is limited to the case of periodic DPHs [20].

We present in Fig. 2(a) a theoretical view of our sample. Each hologram, that targets an angular direction, is sampled in periodic distributions of hoels with a period $\Lambda = 270$ µm and size ω. The DPH is also periodic with a period $\delta = 27$ µm. Due to the ratio $\Lambda/\delta = 10$, the DPH consists of a periodic repetition of a 10×10 hoels basic pattern. We highlight this pattern with a red dotted line in Fig. 2(a). To facilitate the DPH tracking, one hoels distribution is left unrecorded on the drawing.

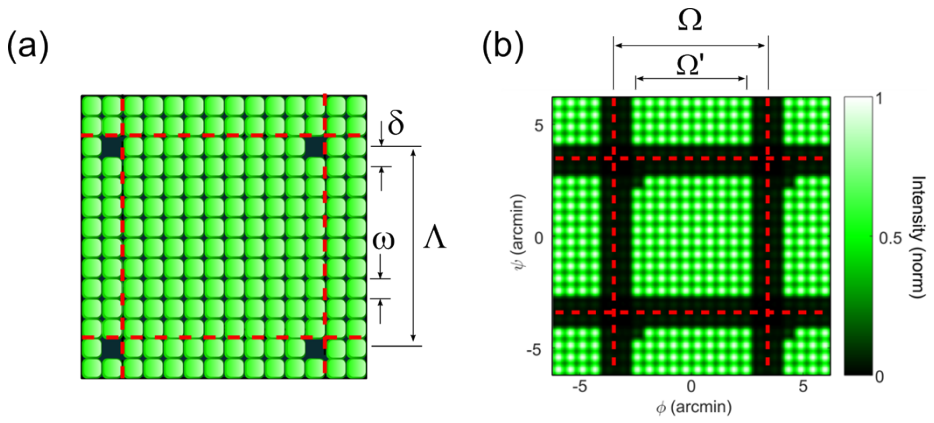

Fig. 2. (a) Graphic representation of the DPH with the size parameters, and (b) simulation of the expected spels distribution resulting from the collective DPH activation.

We present in Fig. 2(b) a simulation of a pattern projected at the focal plane of an optical system when illuminating the sample with a uniform beam. Due to the hoels periodicity, the image projected at the focal plane is also periodic with an angular period given by the grating equation:

$$\Omega = \frac{\lambda}{\Lambda} \tag{1}$$

with λ the wavelength of the beam used to recover the DPH.

Optics EXPRESS

Due to the DPH geometry, we expect an angular repetition of the images with a period $\Omega = 6.8$ arcmin at a wavelength of 532 nm. This value fixes the maximum field of view (FOV) of the DPH, highlighted with red dotted lines in Fig. 2(b). To avoid the overlap of the patterns, we limit the FOV encoded in the DPH to a lower value of $\Omega' = 5.4$ arcmin. The DPHs encode a grid of angular directions in the far field distributed with an angular pitch $\Omega'/10$.

As one hoels distribution has been left unrecorded, one angular direction is missing in the pattern of Fig. 2(b). We locate this missing angular direction in the top left corner of the image. We emphasize that this location in the angular domain is independent of the DPH repartition and could have been located anywhere in the image without any change in Fig. 2(a).

We also would like to emphasize the fact that the image recovery in the far field is related to a controlled reflective effect rather than a simple diffractive effect. Indeed, it is the orientation given to the Bragg gratings during the hoels distribution recording that fixes the angular coordinates. In the focal plane of the optical system, the image recovery is not related to conventional imaging. It is based on an interference effect we call self-focusing, leading to an intensity signal similar to a speckle pattern. In that sense, we don't use the term pixel to describe the elementary image pattern and rather use the term "spel" (elementary spot) to describe each hoels distribution contribution to the image [21].

Diffraction occurs in the imaging process at three main levels:

- Due to the hoels distribution periodicity, images are repeated into various diffraction orders. This strongly limits FOV, and part of our research intends to suppress this diffraction issue with the introduction of randomness in the DPH [22].
- The size of the spel on the imaging plane is given by the numerical aperture of the imaging system (the pupil of the eye in the case of a NED).
- The area of projection coming from each hoels distribution is related to the size ω of the hoel. We have demonstrated that this angular field can be dissociated from the angular coding capacity of the hoels [20].

2.2. Hoel activation set-up

In a former contribution [20], we presented a hoels recovery process based on a uniform illumination of the DPHs. In this work published in 2023, the definition of the spels distribution in the pattern is made by a selective recording of the DPH. We show in Fig. 3(a) this recovery configuration: a uniform laser beam and a selective hoels recording to produce the character "R". This contribution demonstrated our ability to encode angular directions in the DPHs, but not our ability to selectively record each angular direction in each hoels distribution. This present work intends to demonstrate this ability with the use of a hoels activation set-up. We show this new configuration in Fig. 3(b): a selective laser beam illumination and a uniform hoels recording to produce the same character "R".

The dynamic DPHs reading set-up used in this work is represented in Fig. 4(a). We use a diode-pumped solid state (DPSS) green laser source from Oxxius, with same wavelength as the holographic printer set-up (532 nm). This laser is coupled into a polarization-maintaining optical fiber located in front of a collimating lens to create a planar beam. An SLM shapes the beam to introduce the selective lightning of the DPHs. This dynamic mask is imaged onto the sample thanks to a 4-f projection set-up. This kind of setup allows for keeping a planar wavefront on the beam while projecting the addressing pattern. An alignment system is placed behind the sample and provides a visual control for the alignment between the projection of the mask and the DPH of the sample.

The signal is reflected by the holographic sample, creating beams with the angular information associated with each spels. We use a simple imaging system composed of a lens with a focal

Optics EXPRESS

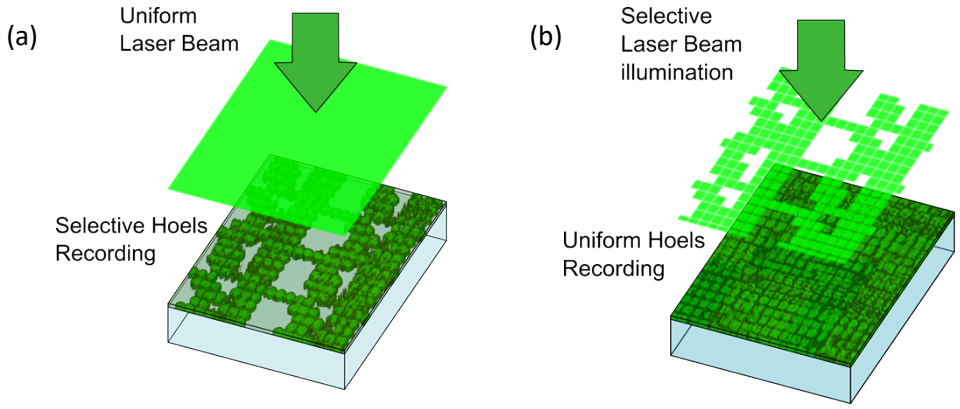

Fig. 3. (a) illustration of a collective DPH activation through uniform illumination, and (b) illustration of a selective DPH activation trough a patterned illumination.

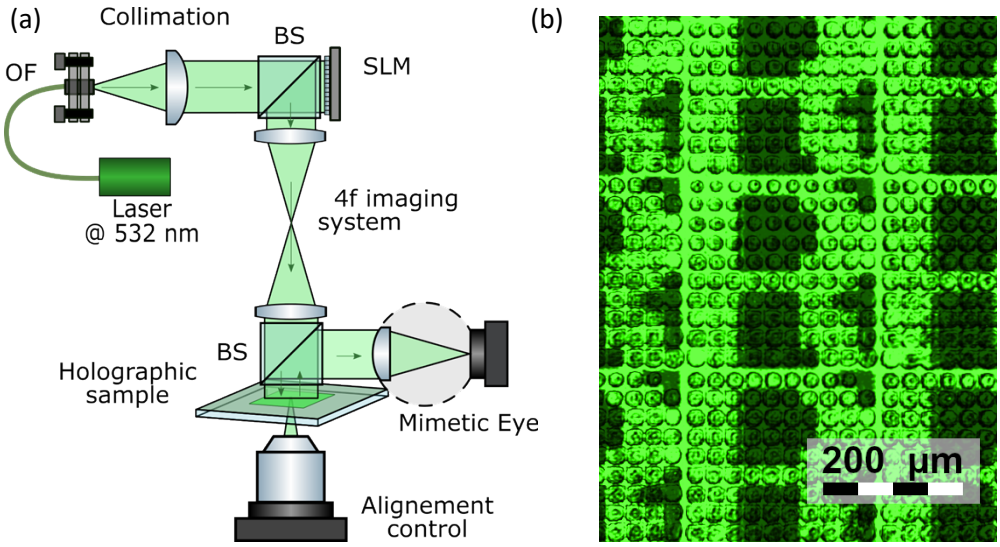

Fig. 4. (a) principle of the optical setup used to activate the hoels (OF: Optical Fiber, BS: Beam Splitter), and (b) image given by the alignment control camera of a DPH pattern projected on the sample (artificially colored in green).

length of 100 mm and a high-resolution camera (UI-1490LE from IDS-imaging) with a pixel size of 1.67 µm and a resolution of 3840×2748 pixels. This imaging system mimics an eye where the lens of the eye projects angular information on the retina.

In this work, the SLM is an LCoS display from Holoeye (HED 6001), configured to work as an amplitude modulator, with a resolution of 1920×1080 pixels and a pixel pitch of 8 µm. The amplitude modulation is encoded on the specular reflexion of the SLM. The diffraction orders, resulting from the SLM pixel grid, occur at angles of about 4°. This sufficiently large angle makes that they do not disturb the image projection in the field of the sample, and the use of a spatial filter in the centre of the 4f system was not required.

One difficulty of the setup concerns the ability to match on the sample both the DPHs and the SLM projected patterns. We make the choice to fix the magnification of the 4f imaging system and to adjust the pattern correspondence by sampling. To set the magnification, we take into

Optics EXPRESS

account the size of the holographic surface, about 6 mm to 8 mm in diameter, and the size of the hoel with $\omega \leq 27$ µm.

Magnification is set to unity with a symmetric 4-f system. Each hoel is sampled over 3×3 pixels on the SLM. With this sampling configuration, the error on the hoel location is limited to ±4 µm, corresponding to less than 15% of the hoel diameter.

We show in Fig. 4(b) a view of the alignment procedure. We see the DPH in transmission mode with the hoels clearly defined as a phase pattern with a circular shape. In this figure, we overlap the SLM pattern to project a character "R" as described in Fig. 3(b). The reader may observe the absence of a hoel located on the top right corner of the DPH distribution. We notice limited deviations in the pattern matching between DPH and SLM illumination. The hoels shape shows some non-uniformity due to non-reproducibility in the hoel recording process [24]. Our goal in this study is to evaluate our ability to selectively and dynamically recover a set of DPHs, with limited crosstalk on the unselected neighbouring DPHs.

3. Results and analysis

3.1. Collective recovery process

A first step consists in analyzing the result of a collective DPH recovery with our setup. This has already been done in our former contribution where we collectively recover a predetermined set of recorded DPH [20]. We showed in this contribution the impact of speckle disturbances and the way to overcome it with averaging of the various diffraction orders. In the current work, we collectively recover the whole set of DPH with our SLM. We show in Fig. 5 the result of the self-focusing on the imaging system over 3×3 diffraction orders.

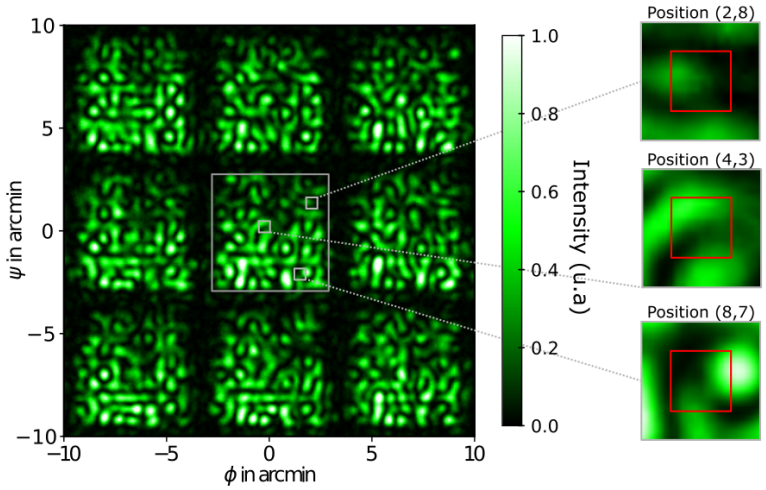

Fig. 5. Measurement of the intensity of a collective DPHs recovery over 3×3 diffraction orders, on the right are the details of the intensity at three pixels locations (pixel surface highlighted with a red square).

The sample projects squares of light with a periodicity consistent with the hoels distribution period of about 6.8 arcmin. The angular size of the squares of about 5.4 arcmin is also consistent with the angular information encoded in the DPH. However, the spels distribution does not correspond to our expectations based on simulations, as shown in Fig. 2(b). This disturbance can be attributed to interferences among the projected spels and to random phase effects in the reflection process of the DPH, resulting in a speckle-like pattern [23]. We show in Fig. 5 (right

Optics EXPRESS

side) three examples of spel intensity at corresponding spel positions. The signal inside each of these pixel locations is neither reproducible nor specific to a spot of light.

To overcome this problem of speckle perturbation, one solution is to perform an average of the intensity among the various diffraction orders [20]. This post-processing step is however not consistent with the concept of dynamic imaging we investigate for the development of a real-time display.

In order to mitigate interferences among the projected spels without post-processing, one can consider two options:

- First is employing different lasers for each hoels distribution. Using distinct lasers in each activation of DPH would eliminate interferences among the projected spels and limits the speckle.
- Second is sequential addressing of the hoels distribution. With sequential addressing of the DPHs, we prevent mutual interferences of spels.

Given the obvious difficulty of using multiple lasers in our optical setup, we investigate the second method.

3.2. *Selective recovery process*

To address the various distribution of hoels using the SLM, we implement a sequential periodic pattern generation on the SLM. Given the disparity in size between the SLM pixels (8 µm) and the hoels ($\omega \leq 27$ µm), we make multiple tests with different configurations of SLM patterns to effectively address the hoels. Following these tests, it was determined that an SLM pattern size of 3×3 pixels (24 µm x 24 µm) allows a good compromise between achieving adequate intensity on each hoel and minimizing crosstalk between the pixels.

In Fig. 6(a) we show an example of spel generation with the activation of one hoels distribution. The activation of a DPH made of a single hoels distribution efficiently generates a spel at a given location. We use the term "pixel" in the projection space to define the squared area corresponding to the periodicity of the projected spels. We show in Fig. 6(b) a crosscut of the intensity at the location of the spel in the horizontal and vertical directions. We observe a good Signal-to-Noise Ratio (SNR) that demonstrates our ability to selectively address the spel. The projection of a single spel avoids the generation of the speckle pattern. We however also observe a dissymmetry in the spel shape.

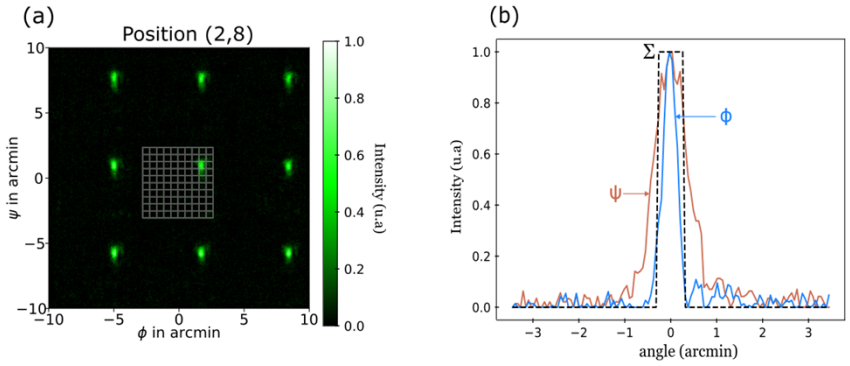

Fig. 6. (a) example of spel projection at location (2,8), the 10×10 grid of pixels is highlighted with gray lines, and (b) cross cut of the intensity at the maximum (horizontal axis ϕ in blue, vertical axis ψ in red), the limits of the pixel surface are highlighted with black dotted lines.

Optics EXPRESS

To evaluate the SNR over the display surface, we integrate the measured intensity over the surface Σ of pixel i,j to calculate its signal level S_{ij} as defined by:

$$S_{ij} = \iint_{\Sigma} I(\psi - \psi_i, \phi - \phi_j) d\psi d\phi \tag{2}$$

we define our SNR as the ratio of energy between a targeted pixel and the neighboring pixels. This SNR estimation is given by the equation:

$$\Gamma_{ij} = \frac{S_{ij}}{mean(S_{pq})_{p,q \in \Xi}} \tag{3}$$

with Ξ a group of pixels neighboring the pixel i,j as represented in Fig. 7(a) and Fig. 7(b).

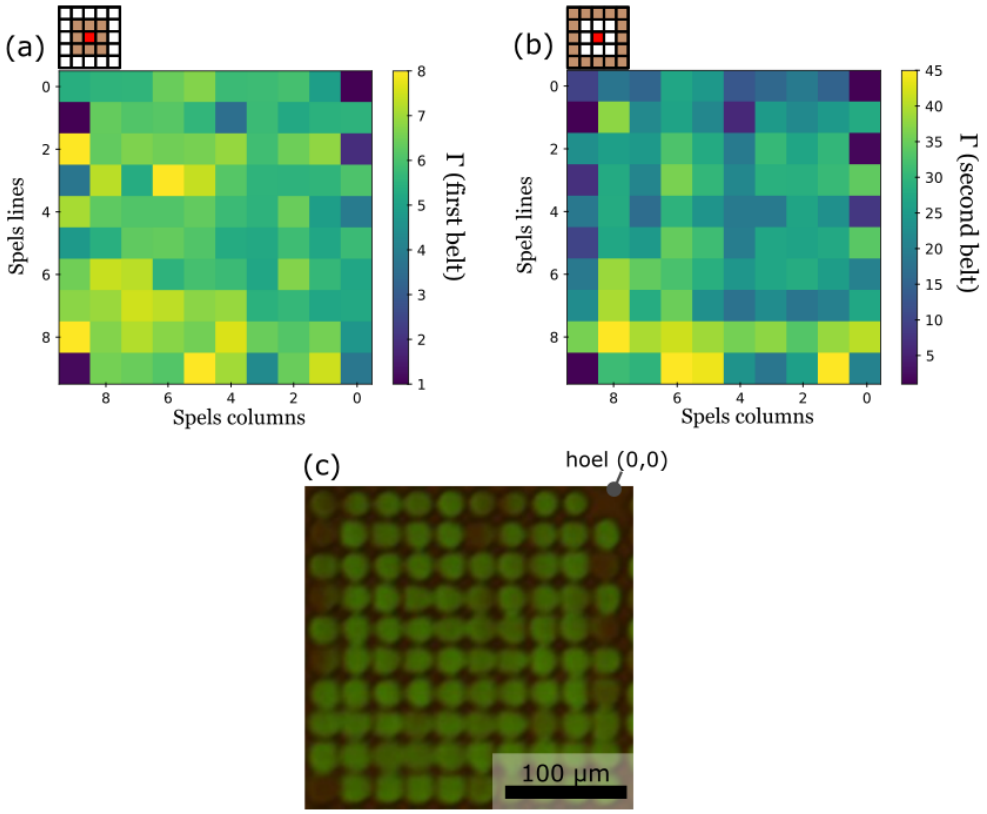

Fig. 7. Distribution of Γ of selective hoels distribution activation for neighboring pixels in the first and second belt of pixels (resp. (a) and (b)), and (c) Microscope photography of the holographic sample taken in reflective mode (real colors) over one 10×10 hoels basic pattern.

We perform calculus of this metric for each spel projection on two sets of neighboring pixels. We report our results in Fig. 7(a) and 7(b) in the case of the belt of 5 closest pixels and of the second belt of 16 pixels. We compare these values with a view of one 10×10 hoels basic pattern. This view, shown in Fig. 7(c) is taken with a microscope working in reflection mode. The photography is in real color and describes the relative efficiency of each hoels distribution. We notice the absence of the unrecorded hoels distribution located on the top right of the pattern.

Optics EXPRESS

We observe some hoels with low efficiency corresponding to defects in the recording process. We attribute these defects to vibration issues as they are often located on the border of the pattern, after a vertical movement of the sample. We reject the defective pixels and calculate the average of the SNR. We measure a mean SNR value of 5.9 with a standard deviation of 1.3 for the closest pixels. The measure on the second belt of pixels gives a higher SNR of about 26.4.

These results lead to two conclusions: the recording process is efficient to record angular information limited to targeted hoels distribution, and we can select individual hoels distributions with good efficiency. The higher crosstalk level measured in the closest pixels might be due to misalignment issues of the addressing pattern, which cause a partial activation of pixels close to the pixel under investigation. We believe that this cross-talk effects could be improved by using better optics, presenting less aberration than a single lens. However, our results are positive and open the way to dynamic image projection without speckle perturbation using sequential activation of DPHs.

3.3. Dynamic recovery

The goal of our investigation is to evaluate new concepts of imaging systems for NED development. In that sense, the evaluation of dynamic pattern projection should be done regarding the visual process with a particular concern on visual and retinal persistence [25]. At this stage, such evaluation cannot be done with a human observer and we perform the analysis of image projection through the integration time of our digital imaging system.

The main constraints of the setup are given by our camera and by the SLM temporal response. The maximum integration time of our camera is 0.5 s (the camera is operating at a frequency of 2 Hz). The SLM has an operating frequency of 60 Hz, corresponding to the period necessary to modify the entire voltage of the pixels composing this SLM.

Considering these values, it is theoretically possible to project an image composed of 30 single spels over a period of 0.5 s. However, in our case, projected spels are efficiently resolved only when a sufficient amount of hoels of the targeted distribution is activated. We describe this issue in Fig. 8. The projection sequence diagram of one spel is represented in Fig. 8(a). It is separated into two periods. In the first period, the pattern to be projected by the SLM is gradually loaded on the LCoS grid. This time period is about 17 ms (1/60 Hz). During the second period, we keep the pattern projection static to generate a steady spel.

The first period corresponds to a progressive formation of the spel. In Fig. 8(b), 8(c), and 8(d) we illustrate the hoel activation (on top) and the corresponding spel formation with a simulation of the interferences (down). When the two first hoels are activated, the self-focusing effect generates a typical Young's interference pattern. Progressively the interference pattern gains in complexity as more hoels are activated. At the end of the first period (Fig. 8(c)) the spel is formed and kept for the second period. The whole projection process occurs at a frequency of about 30 Hz. Considering the integration time of the camera, it limits the number of spels to be projected to a value of about 15.

We evaluate this illumination protocol to project simple patterns composed of 12-13 spels. Figure 9 shows the projections of three different DPHs corresponding to the letters of the CEA research institute. The result is given over 3×3 diffraction orders. We underline that these results are given without post-processing of the images.

The letters are well perceived with a good resolution and visual contrast. We observe a background noise, due to parasitic sources, but also to the signal perceived during the formation of addressing patterns in the first period of the projection process.

3.4. Discussion

These results confirm the ability to selectively and dynamically address sets of DPHs to produce images in a self-focusing imaging process. To our knowledge, it is the first attempt to introduce

Optics EXPRESS

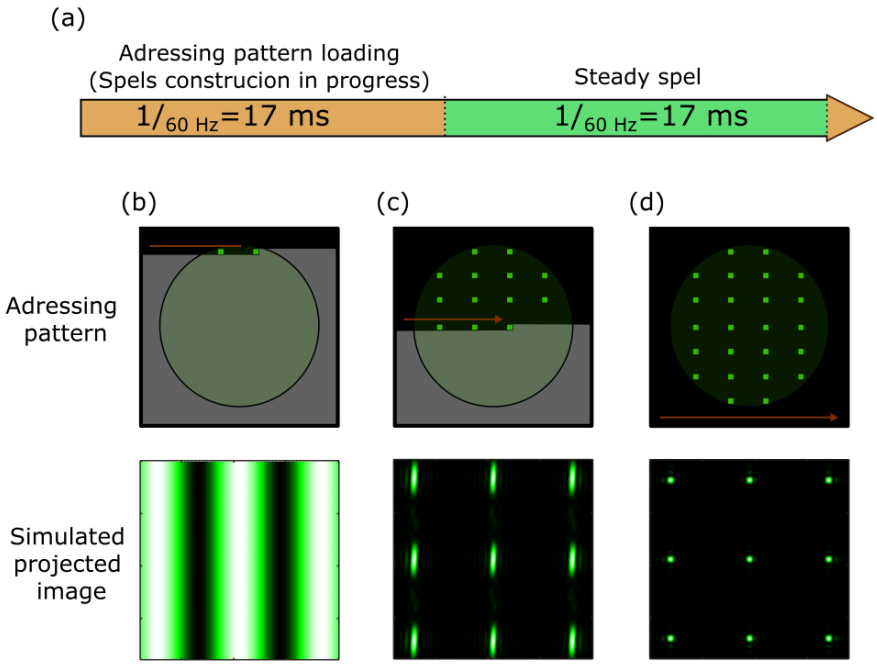

Fig. 8. (a) diagram of one spel projection sequence, (b), (c), and (d) illustration of hoels activation (on top) and the corresponding interference pattern simulated on the camera plane (down).

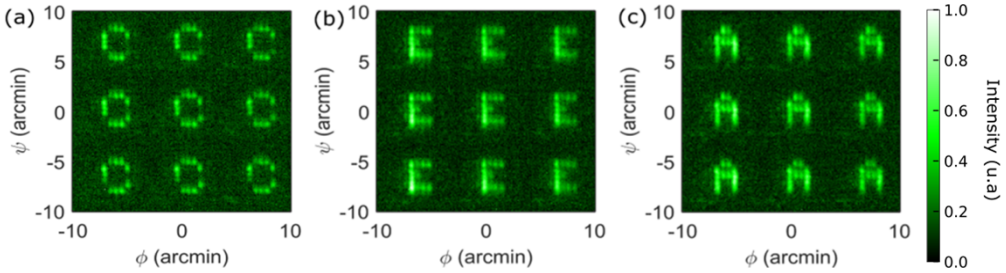

Fig. 9. (a), (b) and (c) Results obtained by carrying a dynamic activation of the DPHs projecting the letters of the text "CEA", using a 30 Hz SLM frequency and a 0.5 s camera integration.

dynamic behavior in a volume holographic photo-material using a hoel concept. This result still lay far from the expected behavior of a user-friendly NED system, but anyway represents a breakthrough in the domain, and a necessary step to validate our disruptive concept of imaging systems based on lens-free auto focalization through the eye.

This first demonstration underlines the main issues to overcome for an efficient display system. The FOV is constrained by the periodicity of the hoels distribution. To increase the FOV we must decrease the hoels distribution pitch Λ (Eq. (1)). But as shown in Fig. 2(a), it leads to the reduction of the number of DPHs for a given hoel size ω. This reduction impacts the number of pixels in the projected image and degrades the quality of the display in terms of resolution. To overcome these limitations on FOV and resolution we must introduce random distribution strategies in the design of the DPHs [22].

Optics EXPRESS

The use of a SLM in a free space setup is here for demonstration purpose, as it strongly constrains the imaging performance in terms of video frequency and can generate unwanted diffraction orders [19]. It also limits the self-focusing effect to the use of a single laser for addressing the DPHs. In the final concept, light is to be channeled to the hoels through a PIC with the use of several lasers. This will allow for both a faster response time and less cross-interference between the spels. The design of this PIC and its manufacturing is very challenging, particularly for the random addressing of the DPHs in the visible range. It represents an active field of research in our laboratory and in the scientific community [26,27].

4. Conclusion and perspective

In this work, we present the first-to-our-knowledge results of dynamic projection using periodic distribution of pixelated holograms. First, we describe the optical free space set-up and the spatial addressing strategy used to activate the DPHs. Preliminary static observations have confirmed the ability to store angular information and to implement the self-focusing effect using our in-house holographic printer. Dynamic projection on selective hoels distributions demonstrates the ability to localize the angular information in these hoels distributions with limited crosstalk. It allows to implement a temporal addressing strategy to project various patterns with the same hoels distributions basis. These results constitute the first step towards a holographic display concept, based on the use of pre-recorded hoels working in reflection, and not presenting diffraction limitations usually associated with the use of SLMs.

In future works, we intend to generalize both the writing and reading process to random distributions of pixelated holograms. We will also pursue investigations on the various aspects of our disruptive near-eye display system, regarding the theoretical imaging behavior related to the display dimensioning, as well as the design and fabrication of an efficient photonic integrated circuit to address the hoels with an optimized device form factor.

Funding. This work was internally funded by CEA-LETI (Laboratoire d'électronique des technologies de l'information).

Acknowledgements. The authors would like to thank both anonymous reviewers for their valuable suggestions to improve the manuscript.

Disclosures. The authors declare no conflicts of interest.

Data availability. Data underlying the results presented in this paper are not publicly available at this time but may be obtained from the authors upon reasonable request.

References

1. H. Bjelkhagen and D. Brotherton-Ratcliffe, *Ultra-Realistic Imaging: Advanced Techniques in Analogue and Digital Colour Holography* (CRC Press, 2013).
2. X. Luo, J. Lawrence, and S. M. Seitz, "Pepper's Cone: An Inexpensive Do-It-Yourself 3D Display," in *Proceedings of the 30th Annual ACM Symposium on User Interface Software and Technology*, UIST '17 (Association for Computing Machinery, 2017), pp. 623–633.
3. D. E. Smalley, E. Nygaard, K. Squire, *et al.*, "A photophoretic-trap volumetric display," Nature **553**(7689), 486–490 (2018).
4. C. Martinez, Y. Lee, N. Clement, *et al.*, "Multi-user volumetric 360° display based on retro-reflective transparent surfaces," Opt. Express **28**(26), 39524–39543 (2020).
5. J. Kim, M. Gopakumar, S. Choi, *et al.*, "Holographic Glasses for Virtual Reality," in *ACM SIGGRAPH 2022 Conference Proceedings*, SIGGRAPH '22 (Association for Computing Machinery, 2022), pp. 1–9.
6. A. Maimone, A. Georgiou, and J. S. Kollin, "Holographic near-eye displays for virtual and augmented reality," ACM Trans. Graph. **36**(4), 1–16 (2017).
7. C. Chang, K. Bang, G. Wetzstein, *et al.*, "Toward the next-generation VR/AR optics: a review of holographic near-eye displays from a human-centric perspective," Optica **7**(11), 1563 (2020).
8. A. W. Lohmann and D. P. Paris, "Binary Fraunhofer Holograms, Generated by Computer," Appl. Opt. **6**(10), 1739–1748 (1967).
9. C. Martinez, F. Laulagnet, and O. Lemonnier, "Gray tone image watermarking with complementary computer generated holography," Opt. Express **21**(13), 15438–15451 (2013).
10. P. Gentet, Y. Gentet, and S. Lee, "An in-house-designed scanner for CHIMERA holograms," in *Practical Holography XXXVII: Displays, Materials, and Applications* (SPIE, 2023), 12445, pp. 79–83.

Optics EXPRESS

11. J. Hofmann, A.-K. Friedel, R. Fiess, *et al.*, "Angle-compensated holographic wave front printing for the fabrication of holographic optical elements operating in the infrared," Opt. Eng. **59**(10), 1 (2020).
12. C. Jang, O. Mercier, K. Bang, *et al.*, "Design and fabrication of freeform holographic optical elements," ACM Trans. Graph. **39**(6), 1–15 (2020).
13. Y. Su, Z. Cai, W. Zou, *et al.*, "Viewing angle enlargement in holographic augmented reality using an off-axis holographic lens," Optik **172**, 462–469 (2018).
14. D. E. Lucchetta, A. Di Donato, G. Singh, *et al.*, "Optically tunable diffraction efficiency by photo-mobile holographic composite polymer material," Opt. Mater. **121**, 111612 (2021).
15. Y. Li, J. Semmen, and S.-T. Wu, "Switchable flat optical elements with patterned cholesteric liquid crystal for augmented reality displays," in *Optical Architectures for Displays and Sensing in Augmented, Virtual, and Mixed Reality (AR, VR, MR) IV* (SPIE, 2023), 12449, pp. 134–143.
16. S. Fenoll, F. Brocal, J. D. Segura, *et al.*, "Holographic Characteristics of Photopolymers Containing Different Mixtures of Nematic Liquid Crystals," Polymers **11**(2), 325 (2019).
17. P.-A. Blanche, A. Bablumian, R. Voorakaranam, *et al.*, "Holographic three-dimensional telepresence using large-area photorefractive polymer," Nature **468**(7320), 80–83 (2010).
18. C. Martinez, V. Krotov, B. Meynard, *et al.*, "See-through holographic retinal projection display concept," Optica **5**(10), 1200–1209 (2018).
19. S. Moser, M. Ritsch-Marte, and G. Thalhammer, "Model-based compensation of pixel crosstalk in liquid crystal spatial light modulators," Opt. Express **27**(18), 25046–25063 (2019).
20. C. Martinez, M. Colard, P. Legentil, *et al.*, "Sparse holographic imaging for an integrated augmented reality near-eye display," Appl. Opt. **62**(8), 1928–1938 (2023).
21. V. Krotov, C. Martinez, and O. Haeberlé, "Experimental validation of self-focusing image formation for retinal projection display," Opt. Express **27**(15), 20632–20648 (2019).
22. F. Rainouard, M. Colard, O. Haeberlé, *et al.*, "Optimal dense and random addressing design of emissive points in a retinal projection device," in *Optics, Photonics and Digital Technologies for Imaging Applications VII* (SPIE, 2022), 12138, pp. 199–208.
23. F. Rainouard, M. Colard, O. Haeberle, *et al.*, "Simulation of speckle in pixelated hologram image recovery: application for augmented-reality retinal projection device," in *Practical Holography XXXVII: Displays, Materials, and Applications* (SPIE, 2023), 12445, pp. 64–71.
24. P. Legentil, C. Bereyziat, M. Colard, *et al.*, "Development of pixelated holograms recording strategies and aging study of different holographic photopolymer mechanisms for Augmented Reality applications," in *Practical Holography XXXVI: Displays, Materials, and Applications* (SPIE, 2022), 12026, pp. 17–25.
25. Y. Galifret, "Visual persistence and cinema?" C. R. Biol. **329**(5-6), 369–385 (2006).
26. K. Millard, F. Rainouard, D. Fowler, *et al.*, "Multilayer photonic-integrated circuit design for dense random waveguide distribution addressing, application to near-eye display," in *Optical Architectures for Displays and Sensing in Augmented, Virtual, and Mixed Reality (AR, VR, MR) IV* (SPIE, 2023), 12449, pp. 144–151.
27. J. K. S. Poon, A. Govdeli, A. Sharma, *et al.*, "Silicon photonics for the visible and near-infrared spectrum," Adv. Opt. Photonics **16**(1), 1–59 (2024).